In-operando Quantification of Electrode Flooding in CO_2 Electrolysis and Correlation to Product Distribution

[z]Daniel Rottmann[1,2], Ricarda Kollmuss[1], Stefan Haufe[1], Karl J. J. Mayrhofer[2,3]

Affiliations:
[1]Wacker Chemie AG, Consortium für elektrochemische Industrie, Zielstattstr. 20, 81379 Munich, Germany
[2]Department of Chemical and Biological Engineering, Friedrich-Alexander University Erlangen-Nürnberg, Cauerst. 1, 91058, Erlangen, Germany
[3]Helmholtz Institute Erlangen-Nürnberg for RenewableEnergy (IEK-11), Forschungszentrum Jülich GmbH, Cauerst. 1, 91058 Erlangen (Germany)

[z]Corresponding Author E-mail Address: daniel.rottmann@wacker.com

Abstract

Flooding of the gas diffusion electrode (GDE) is one of the most important failure mechanisms limiting the long-term stability of CO_2 electrolysis. Methods to characterize the GDE flooding process during the electrochemical reduction of CO_2 are essential in order to improve the understanding of this failure mechanism and to consequently accomplish a steady performance at industrially relevant operation conditions. Here, a method for in-operando quantification of GDE flooding is presented. By collecting and weighing the amount of electrolyte which leaked through the GDE of a flow cell electrolyzer, utilizing a water trap on a balance, a time-resolved correlation between flooding data and product distribution is obtained. To demonstrate its potential, the in-operando weighting is used to determine leakage rates under dynamic and static CO_2 electrolysis conditions and correlate them with the distribution of the gaseous reaction products. This new technique provides a deeper understanding of the dynamic processes behind GDE flooding during CO_2 electrolysis and its influence on the product distribution, enabling the development of novel mitigation strategies.

Introduction

The constant increase in atmospheric CO_2 concentration and the concomitant global warming are highly pressing societal challenges[1,2]. In this context, the electrochemical reduction of CO_2 has emerged as an attractive opportunity to reduce CO_2 emissions, while also storing renewable energy into value-added platform chemicals[3,4]. However, up to this day the

industrial feasibility for CO_2 electrolysis has not been reached. While the upper ranges of typically reported current densities and faradaic efficiencies (FE) towards CO and C_2H_4 are already within the industrially relevant range, most systems achieve only a couple of hours lifetime in contrast to 10,000 to 90,000 hours of operation required for economic feasibility[5-8].

This insufficient lifetime can have several reasons, one major origin is the instability of the gas diffusion electrode (GDE) that leads to a decay in CO_2 conversion ability after only a couple of hours[8,9]. GDEs usually consist of a porous gas diffusion layer (GDL) bearing a catalyst layer (CL) on top[10]. In theory, the GDE´s porous structure should maintain a stable three-phase boundary between the gaseous reactant, the liquid electrolyte, and the solid catalyst. This boundary minimizes CO_2 mass transport limitations to the CL and enables operation at industrially relevant current densities (>100 mA cm^{-2})[6,11]. However, especially at medium to high current densities, the liquid electrolyte can quickly flood the GDE pores, shifting the gas-liquid interface over time and consequently leading to reduced CO_2 availability at the CL. In parallel, a gradual shift from the CO_2 reduction reaction (CO2RR) to the hydrogen evolution reaction (HER) can often be observed[12].

To date, mitigation of flooding remains a challenge for long-term CO_2 electrolysis, despite identifying multiple reasons for GDE flooding such as electrowetting[12], carbonate salt precipitation[13,14], polytetrafluorethylene (PTFE) degradation[15], uneven pressure distribution across the GDE[16] and liquid product formation[17]. Possible mitigation strategies include, for example, enhancing the CL´s hydrophobicity with PTFE additives to avoid pore intrusion by the aqueous electrolyte or minimizing the carbonate salt precipitation inside the GDE by increasing the humidity of CO_2 or choosing cations with high solubility[8,13,18,19]. While these strategies showed remarkable success in improving system lifetime, GDE flooding could not be mitigated sufficiently to achieve the industrially required stability, thus rendering further understanding of the GDE flooding mechanism necessary.

Recently, Jiang *et al.* classified the relevant characterization methods into two categories. Ex

situ methods for observing and quantifying flooding are focused on the detection of residual salts in the GDE post CO_2 electrolysis, predominately by determining the amount and position of alkali metal cations inside the GDE[20].

Multiple methods such as microcomputed tomography (Micro-CT)[13], scanning electron microscopy (SEM)[13], energy-dispersive X-ray spectroscopy (EDX)[21] and inductively coupled plasma mass spectrometry (ICP-MS)[22] were used to determine the salt distribution inside the GDE after the experiment. These methods achieved great progress in advancing our understanding of GDE flooding.

In situ strategies, on the other hand, provide data in real time and thus also on the dynamics of flooding[20]. Photographing the GDE's gas side during CO_2 electrolysis allowed to observe the formation of electrolyte droplets over time, therefore visualizing the continuous flooding process[23].

Seeking to monitor flooding within the GDE´s porous structure, Disch *et al.* used high resolution neutron imaging on their zero-gap electrolyzer. In this way, not only the electrolyte transport, but also the salt precipitation inside the GDE could be observed over time[24].

To enhance the understanding of the flooding process, it is essential to complement visualization with quantification. One possible method for quantification are double-layer (DL) capacitance measurements. These measurements are based on the assumption of a proportional increase in the electrochemical DL with continuous flooding of the GDE, as more electrode surface gets in contact with the electrolyte[25,26]. While these measurements can quantify the degree of flooding over time, they require interruption of the CO_2 electrolysis to perform cyclic voltammetry[27,28].

Another approach is to measure the electrolyte leaked during electrolysis, which can be carried out without interrupting the electrolysis process. For this method a water trap is placed at the cathode´s gas side outlet, which continuously collects the electrolyte leaked during CO2RR. After electrolysis is complete, the collected electrolyte is weighed and an average leakage rate (weight of electrolyte leakage over time [mg/min], Equation 4) is determined, which correlates with the flooding behavior of the GDE [29,30]. Wrobel *et al.* were able to measure time resolved leakage rates by quantifying the collected electrolyte every two hours by removing

the collection vessel from the system and placing it onto a scale. A simultaneous determination of the product FEs and the GDE leakage rate is, however, difficult with this setup, as the quantification of the gaseous products is interrupted during the quantification of the leaked electrolyte [31].

In this work we present an in-operando water trap that overcomes this problem and combines the following unique features: 1) in-operando quantification of GDE flooding by determining time resolved leakage rates and 2) simultaneous quantification of gaseous products.

Experimental

Electrolysis setup: A Micro Flow Cell® (ElectroCell) was used for all CO_2 electrolysis experiments. The cell consists of a gas, a catholyte and an anolyte compartment. Catholyte and anolyte were separated by a bipolar membrane (Fumasep® FBM, FUMATECH BWT), whereas the gas and catholyte compartment were separated by the cathode/GDE (geometric area 5 cm^2). For the anode an Ir-MMO plate (ElectroCell, geometric area of 10 cm^2) was used.
Both catholyte and anolyte consisted of 220 ml 1 M KOH (Sigma-Aldrich, ACS reagent) prepared with ultrapure water (Arium® mini, Sartorius) and were recirculated through the cell with micro gear pumps. The catholyte was recirculated at 5 ml min^{-1} and the anolyte at 33 ml min^{-1}. The CO_2 (Linde, quality 2.5) volume flow was controlled with a mass flow controller (Bronkhorst, El-Flow select) and was held constant at 40 ml min^{-1}.

GDE preparation: The GDE cathode was prepared by coating a 13.5 x 13.5 cm^2 gas diffusion layer (Freudenberg, H23C8) with a catalyst ink containing Cu nanoparticles (Sigma-Aldrich, 40-60 nm) and Nafion™ (Ion Power, 20 wt.%) in an 88:12 mass ratio. In detail, 451 mg Cu nanoparticles and 278 µL Nafion™ were first finely dispersed in an isopropanol/water (50 ml, 50:50 by volume) mixture using an ultrasonic horn (Hielscher, UIS250v) for 30 min, while the mixture is continuously cooled with an ice bath. Afterwards, the catalyst ink was coated onto the GDE using a home-built inkjet printing system until a mass loading of 0.8 mg cm^{-2} was reached. The inkjet printer consisted of an inkjet printing unit (Vermes, MDS1560 equipped

with a ceramic pestle CTF 4) connected to an xyz-plotter (imes-icore, ICV 4030 xyz). The catalyst ink is continuously recirculated through the printing unit by a micro gear pump at 350 ml min^{-1} to avoid ink sedimentation during the printing process. In addition, the catalyst ink is under 0.2 bar nitrogen pressure to prevent unwanted Cu oxidation and to keep the hydrostatic pressure constant. The GDL is placed on an aluminum plate temperature-controlled to 90 °C underneath the printing unit. The printing unit moves in serpentine patterns over the GDL area, while small suspension droplets are propelled at 41 Hz from the printing unit onto the GDL, where the solvent evaporates immediately. The final loading is controlled by the number of printing runs on the GDL.

Electrochemical procedure: The electrolysis cell was operated galvanostatically using a potentiostat (BioLogic, SP150-E + 20 A booster). Before each experiment, the cell was equilibrated for 4 min at open circuit voltage (OCV) while CO_2 gas and electrolytes were flowing. Thereafter, the current density was increased via linear sweep amperometry (LSA) at a ramp of 2 mA s^{-1} cm^{-2} until the desired current density for chronopotentiometry is reached. After reaching the desired current density, chronopotentiometry is applied and the quantification of the gas product and the percolation rate starts.

Quantification of liquid products: Nuclear magnetic resonance (NMR) spectroscopy was used to quantify liquid CO2RR products (ethanol, propanol, acetic acid, formic acid) at the end of an experiment within the catholyte. Measurements were conducted with an Avance III HD 500 MHz (Bruker) NMR spectrometer equipped with a SampleXpress autosampler. Each catholyte sample is measured twice with two different internal standards. Liquid products upfield of the water signal were referenced to the sodium trimethylsilylpropanesulfonate (DSS) as internal standard, while peaks downfield of the water signal were referenced to the potassium hydrogen phthalate (KHP) as internal standard. In detail, 540 µl catholyte was taken after the experiment and mixed with 60 µl internal standard (either 0.1 mg mL^{-1} DSS or 1.0 mg ml^{-1} KHP solved in D_2O) to have an overall sample volume of 600 µl. The samples were measured with the water suppression pulse sequence noesygppr1d (1D NOESY with pre-saturation and spoil gradients)

to suppress the water peak and facilitate evaluation. One experiment consisted of 64 scans with a delay time (d1) of 60 seconds to ensure quantitative relaxation of all relevant nuclei.

Quantification of gaseous products and leakage: Gas chromatography is used for the quantification of gaseous products and their respective volumetric gas flow ($\dot{V}_{prod}$). A gas chromatograph (8860, Agilent, modified by Joint Analytical Systems GmbH) equipped with a thermal conductivity detector is used to quantify the concentrations and the gas flow of the gaseous products. Using Helium (Linde, quality 5.0) as a carrier gas and three serially connected columns (Hayesep Q, HP-PLOT-Q, HP-PLOT 5A), an automated injection, separation and quantification of the product gas stream is possible every 9.5 min.

The product gas flow ($\dot{V}_{prod}$) is determined by dosing an additional N_2 volume flow ($\dot{V}_{N2}$, 20 ml min^{-1}) into the product gas stream shortly before the GC. This N_2 volume flow acts as an internal standard and allows to determine $\dot{V}_{prod}$ according to the following equation:

$$\dot{\boldsymbol{V}}_{\boldsymbol{prod}} = \frac{\dot{\boldsymbol{V}}_{\boldsymbol{N2}}}{\boldsymbol{\varphi}_{\boldsymbol{N2}}} - \dot{\boldsymbol{V}}_{\boldsymbol{N2}} \tag{1}$$

with φ_{N2} being the the volume fraction of N_2 within the product gas flow. Note that the GC was calibrated with N_2/Ar gas mixtures between 1-100 vol. % to ensure correct N_2 quantification (see Figure S2 in SI). These mixtures were prepared with mass flow controllers (Bronkhorst, El-Flow select), which were prior calibrated with a DryCal (Mesalabs, FlexCal). The GC calibration for CO_2 electrolysis products was accomplished by injecting calibration gases (Tyczka Industrie-Gase GmbH) including the following components: CH_4, C_2H_6, C_2H_4, CO, H_2 and CO_2. The different calibration points were obtained by diluting the initial calibration gas and are depicted in Figure S3 This allows to determine the FEs of the individual gaseous products:

$$\boldsymbol{FE_i} = \frac{\boldsymbol{\varphi_i} \times \dot{\boldsymbol{V}}_{\boldsymbol{prod}} \times \boldsymbol{F} \times \boldsymbol{z_i}}{\boldsymbol{V_M} \times \boldsymbol{I}} \times \mathbf{100}\,\% \tag{2}$$

With F being the Faraday constant (96,485 $\frac{C}{mol}$), z being the stochiometric number of

electrons consumed for the individual product, V_M being the molar volume of an ideal gas (22.41 $\frac{l}{mol}$), I being the applied current and φ_i being the volume fraction inside the product gas stream of the individual products. Note that volume fractions of product gases quantified by the GC ($\varphi_{i,N2\ diluted}$) need to consider the dilution by the internal N_2 standard. A conversion can be carried out by Equation (3):

$$\boldsymbol{\varphi_i = \frac{\varphi_{i,N2\ diluted} \times (\dot{V}_{prod} + \dot{V}_{N2})}{\dot{V}_{N2}}} \quad (3)$$

Quantification of leakage was performed using an analytical tuning fork balance (Kern & Sohn, PNS3000-2). The complete setup is depicted in Figure 1: Electrolyte droplets formed on the backside of the GDE are being pulled by gravitational force and gas flow towards the water trap. The water trap is positioned below and slightly offset of the electrolyzer cell, which allows electrolyte droplets to move via gravitational force towards the water trap. It is connected to the cathode's gas outlet via flexible tubing (PROLIQUID, TYGON A-60-C). The analytical balance measures the amount of leaked electrolyte every minute as soon as the chronopotentiometry has started. This allows to calculate leakage rates over the experiment´s course:

$$\boldsymbol{Leakage\ rate = \frac{\Delta m}{t}} \quad (4)$$

With Δm being the collected mass of electrolyte [mg] during the time period and t being the length of the period [min].

According to the calibration certificate, the analytical balance has a measurement uncertainty of ±10 mg, which translates to an uncertainty of ±0.4 mg min^{-1} for leakage rates over a time-intervall of 30 min. To assess the stability of the scale over time we conducted a control experiment where the scale was operated for 800 minutes under the same conditions as the leakage experiments but without electrolysis taking place (no electrolyte droplets in the collection vessel). Over this period, the scale showed an erroneous increase of 100 mg, corresponding to a drift rate of ±0.2 mg min^{-1}. In total we estimate our uncertainty of leackage measurements around ±0.6 mg min^{-1} which is small relative to the total mass changes observed in our experiments (see Figure 2). To avoid misinterpreting fluctuations caused by the water

trap's error (~10 mg) as collected electrolyte, only changes of at least 100 mg were considered significant.

Results and Discussion

Simultaneous quantification of gaseous products and leakage rates is achieved by connecting a flow cell in series with a water trap standing on a scale, followed by an online gas chromatograph (GC). A schematic drawing of the in-operando water trap setup is shown in Figure 1. Electrolyte droplets, formed on the gas side of the GDE by leakage during CO2RR, are drawn by gravitational force and the product gas stream towards the water trap. The water trap is placed below and slightly offset to the electrolyzer cell and it is connected to the cathode's gas outlet via flexible tubing. A laboratory scale is continuously measuring the amount of accumulated electrolyte inside the water trap, while CO_2 and its gaseous reduction products leave the collection vessel and are directed towards a gas chromatograph (GC) for periodic quantification of the gaseous reduction products.

To ensure proper quantification of the liquid leakage in the water trap, it is important to utilize flexible tubing (see Experimental for detailed description) connecting the collection vessel to the electrolysis cell and the GC. If there is tensile stress on the tubing, a continuous weight drift of the scale might be observed. Furthermore, the tubing should be fixated to prevent its movement or vibration, as this would manifest as strong fluctuations in the determined mass. This is especially important when working in an area with ventilation, such as a fume hood. Finally, the collection vessel should be placed centric on the scale to ensure correct quantification.

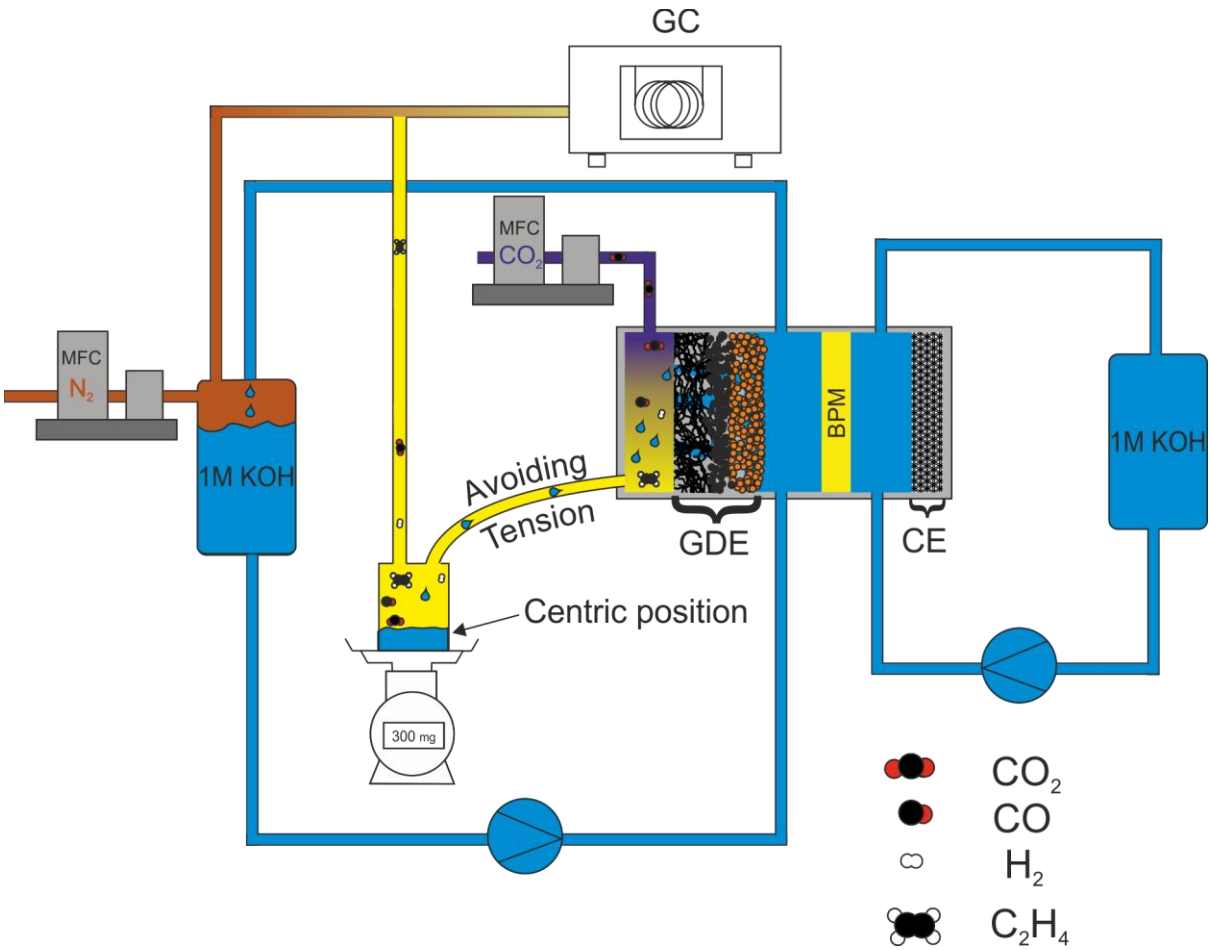

Figure 1 Schematic process scheme with implemented in-operando water trap. Electrolyte droplets, formed by the GDE flooding process, are continuously quantified when entering the collecting vessel, while the distribution of the gaseous reduction products is monitored by GC injections.

To show the potential of the developed technique, first, the GDE flooding on Cu GDEs was investigated during galvanostatic conditions between 100 and 300 mA cm^{-2} in aqueous electrolyte (1 M KOH) for 4 hours. The electrolyte leakage through the GDE is quantified every minute, and in parallel the gaseous production distribution is determined every 9.5 min by a GC. Average percolation rates over 30-minute time intervals are calculated according to Equation 4 (see Experimental). It should be noted that time intervals for calculations should be chosen according to the accuracy of the balance (here ±10 mg). The time-resolved percolation rates and gaseous product FEs are depicted in Figure 2 for the different current densities.

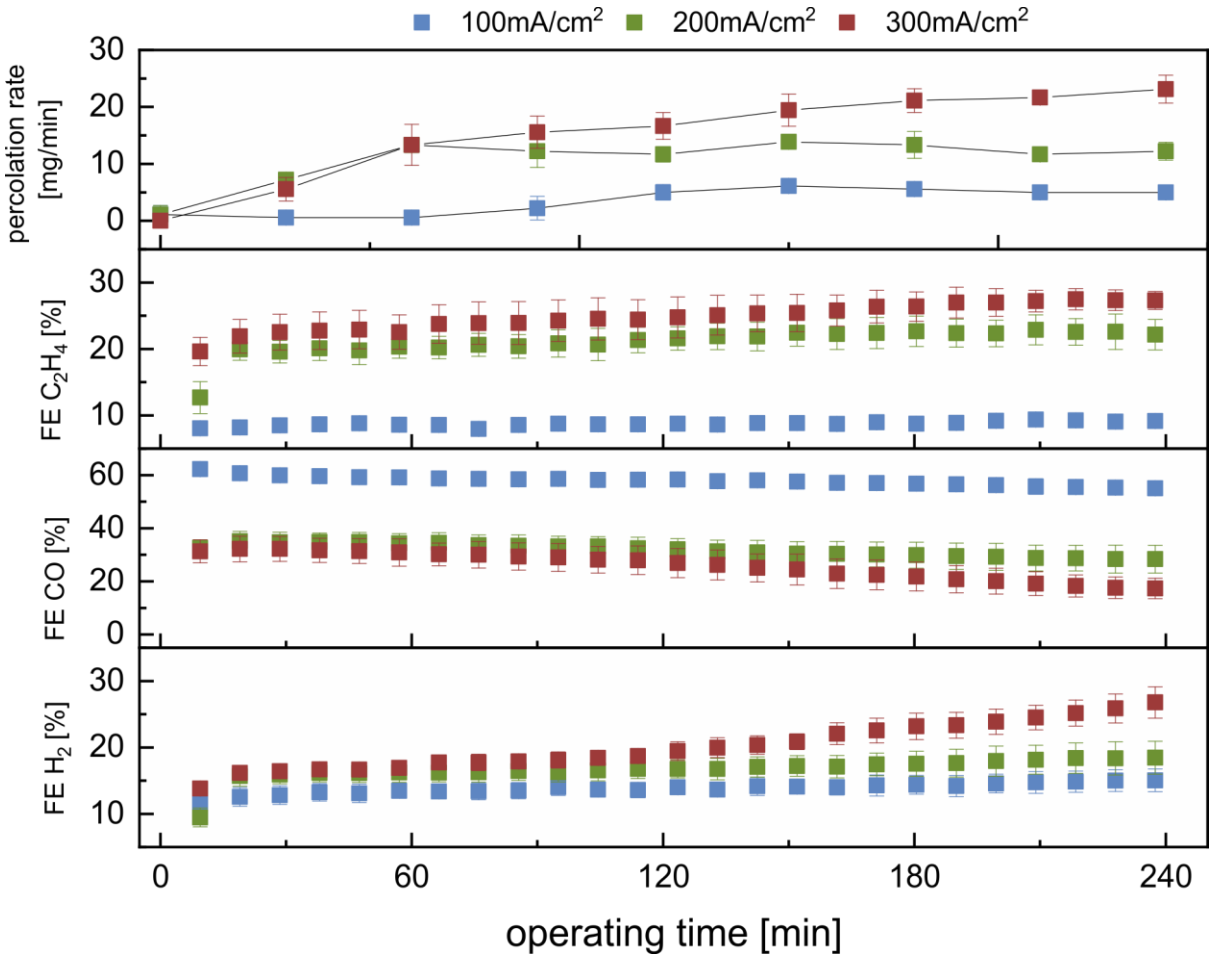

Figure 2 Temporal progression of FE_{C2H4}, FE_{CO}, FE_{H2} and percolation rates (weight of electrolyte leakage over time) during galvanostatic CO_2 reduction on a Cu-based GDE at current densities of 100 mA cm^{-2}, 200 mA cm^{-2} and 300 mA cm^{-2}. Each experiment is repeated twice, with error bars to indicate the standard deviation. The estimated error of ±0.6 mg min^{-1} for the in-operando water trap system is small compared to the experimental standard deviations of 0.8 – 3.5 mg min^{-1}. This suggests that the variability of the experimental results is dominated by other factors such as GDE coating or assembly of the electrolysis cell. Gaseous product distribution and leakage rates over time indicate a current and time dependent GDE flooding.

By using the in-operando water trap, it is observed that the leakage rates during 200 and 300 mA cm^{-2} experiments are increasing over time, while the percolation rate at 100 mA cm^{-2} seems to be constant and less pronounced throughout the experiment's course. While it is known that the FEs can change over time due to GDE flooding[23], it can now be observed

that the percolation rate also changes during galvanostatic measurements. Interestingly, the leakage rates at 200 and 300 mA cm^{-2} are quite similar up to approx. 120 min, with the percolation rate increasing further at 300 mA cm^{-2}, while the rate remains constant during the 200 mA cm^{-2} experiment. Increasing percolation rates could indicate a time dependent degradation of the GDE and therefore loss of hydrophobicity. The degradation mechanism also might be current dependent since higher current densities lead to a faster increase in leakage.

By comparing the carbonaceous products, it is observed that current densities beyond 100 mA cm^{-2} lead to a significant increase in FE_{C2H4}. This increase is visible from the start and is expected as higher current densities lead to more dimerization of CO* species adsorbed on the catalyst's surface, consequently shifting the FE from CO to C_2H_4[7,32]. Regarding the FE_{H2} only a comparable small current density dependency can be observed in the first 120 min. However, after roughly 120 min the FE_{H2} of the experiment at 300 mA cm^{-2} shows a significant increase in comparison to the experiments with the other current densities.

Correlating percolation rates and FE_{H2}, one can observe that a time and current dependent flooding of the GDE takes place. The highest current density (300 mA cm^{-2}) showed the highest percolation rates after 120 min, which was accompanied by an increase in the FE_{H2}. This suggests that the GDE degradation is most dominant at 300 mA cm^{-2} and it took approximately 120 min for the degradation to lead to increased flooding. This flooding was evident by a shift from CO_2 conversion to the HER.

One possible degradation mechanism could be the carbonation of the electrolyte, which leads to the precipitation of carbonate salts in the GDE[13]. Carbonation occurs through the neutralization of KOH with CO_2 from the gas stream, which can be observed by a pH shift. While all experiments start at a pH of 14 (1 M KOH), we noticed different pH shifts depending on the current density. At a current density of 100 mA cm^{-2}, the electrolyte remains strongly alkaline at the end of electrolysis after 4 h, with a pH value of 13.87 ± 0.02. In contrast, at 200 mA cm^{-2}, the pH value decreases slightly to 13.51 ± 0.03, and at 300 mA cm^{-2}, it drops significantly to 11.12 ± 0.09. These pH shifts indicate that carbonate formation increases with higher current density. This hypothesis is further supported by the cell voltages, which increase at varying rates depending on the current density (see Figure S4). The behavior can be

explained by the increasing electrolyte resistance caused by carbonation. As the leakage rates of the GDEs rise with increasing current density, the carbonation of the electrolyte and the resulting precipitation of carbonate salts in the GDE may accelerate flooding. However, further investigations are needed to confirm this hypothesis, as other potential causes of GDE flooding may also be influenced by current density.

Another potential contributor to GDE flooding is the accumulation of liquid products and the consequent surface tension reduction by alcohols during electrolysis. To quantify the accumulation of liquid products, NMR spectroscopy was used to determine the liquid product concentrations at the end of each experiment. The average partial current densities for the various liquid products over the course of the experiments are shown in Figure 3.

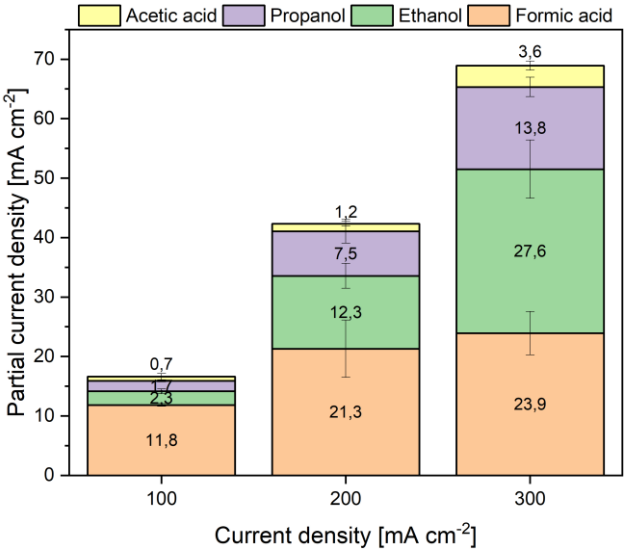

Figure 3 Average partial current densities of liquid products at different current densities. Each measurement is based on the average of three experiment with error bars to indicate the standard deviation. The formation of alcohols is most dominant at 300 mA cm^{-2}.

The results from Figure 3 show that the highest partial current densities for ethanol (approx. 28 mA cm^{-2}) and propanol (approx. 14 mA cm^{-2}) were observed during CO_2 electrolysis at 300 mA cm^{-2}. This corresponds to maximum final concentrations of approximately 0.0052 mol L^{-1} for ethanol and 0.0017 mol L^{-1} for propanol. In comparison, Sahin *et al.* investigated GDE flooding caused by liquid product formation and observed only a minor decline in stability with initial ethanol and propanol concentrations of 0.5 mol L^{-1} and

0.2 mol L^{-1}, respectively[17]. Since our concentrations are significantly lower than those reported by Sahin *et al.*, we assume that the liquid product formation did not significantly contribute to GDE flooding during our experiments.

In a further series (Figure 4), the current density is set to 100 mA cm^{-2} and maintained for a duration of 120 min. Three current density segments are then applied: 200 mA cm^{-2}, 300 mA cm^{-2} and 100 mA cm^{-2}. Within each of these segments, the respective current density is held constant for 60 min. Leakage rates are calculated over each individual current density segment (60 min) plus five additional minutes. These 5 min consider the delay time between the cell and the collecting vessel, as percolated electrolyte first needs to move through the gas compartment and tubing, before quantification inside the collecting vessel takes place (see Figure S1). It should be noted that this estimation could be further improved by monitoring the gas side of the GDE, allowing to follow the movement of percolated electrolyte more closely. NMR was not used to quantify liquid products at the end of an experiment as this method does not provide time-resoluted data, making it impossible to determine the FEs of liquid products for the individual current density regions.

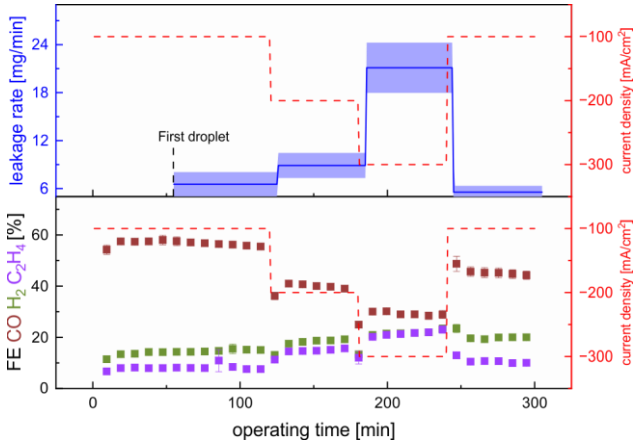

Figure 4 Temporal progression of gaseous product FEs and leakage rates during CO_2 electrolysis with dynamic current density segments ranging from 100 mA cm^{-2} to 300 mA cm^{-2}. Each experiment is repeated twice, with the error bars to indicate the standard deviation. The GDE's state of flooding cannot always be described by the leakage rate alone and needs to be correlated with the FE_{H2}.

Results in Figure 3 show that changing current densities are again accompanied by corresponding changes in percolation rates and FEs. In comparison to the galvanostatic experiments in Figure 2, leakage at 200 mA cm^{-2} (120-180 min) is less pronounced and shows similar values (around 9 mg min^{-1}) to the initial percolation in Figure 2 at 200 mA cm^{-2} (0-30 min at around 7 mg min^{-1}). This observation was not expected, as the results from Figure 2 indicate a time dependent degradation. Consequently, in Figure 3, the percolation rate should have been higher between 120-180 min than between 0-60 min. Similar observations are made when comparing the first and final segment (both at 100 mA cm^{-2}) of Figure 3. Both segments show similar leakage rates (at around 6-7 mg min^{-1}), even though the 200 and 300 mA cm^{-2} segments in between should have increased GDE degradation and leakage rates. This suggests that the causal chain for galvanostatic experiments stated previously (higher current densities lead to more degradation over time and in return higher leakage rates) cannot be applied during dynamic current density CO_2 electrolysis procedures. This result further underlines the complexity behind GDE flooding.

It is also noteworthy that the FE_{H2} in the second 100 mA cm^{-2} segment is approx. 5-6 % higher than in the first 100 mA cm^{-2} segment, despite similar percolation rates. This reveals that the percolation rate alone cannot depict the GDE´s flooding state. Due to the higher FE_{H2}, but similar percolation rates, it could be assumed that more regions of the CL are flooded in the second segment, but these did not contribute to the percolation rate.

Overall, the in-operando water trap can also be used to study the GDE flooding behavior of a cell system during dynamic operation. The investigations clearly show that the flooding status of the GDE cannot always be described by the leakage rate alone but must be correlated with the gaseous product distribution. It also seems that leakage rates are not always directly depending on the GDE´s degradation state, which emphasizes the complexity of the flooding.

In a further experiment, leakage rates and gaseous product FEs are determined while the current density is alternated between 300 mA cm^{-2} and 0 mA cm^{-2} within the experiment (Figure 5). In detail, the current density was set to 300 mA cm^{-2} for 120 min followed by 60 min of open

circuit voltage (OCV) and again 300 mA cm^{-2} for 65 min. The regeneration phase (OCV) was set after 120 min, since galvanostatic experiments at 300 mA cm^{-2} (Figure 2) showed an increase in FE_{H2} and leakage rates at this point in time. During the OCV period, neither the CO_2 volume flow nor the electrolyte circulation are turned off in order to maintain similar process conditions between the electrolysis and regeneration phase. The leakage rates are averaged over three 60 min time periods before, after and during the OCV. It should be noted that time intervals for leakage rates (blue line Figure 5) again consider a 5 min delay time between the electrolysis cell and the collecting vessel (see Figure S1). For example, while the OCV segment is set between 120-180 min, its percolation rate is calculated from 125-185 min to ensure that all electrolyte droplets from the previous segment (0-120 min at 300 mA cm^{-2}) have been purged and do not contribute to the OCV`s percolation rate.

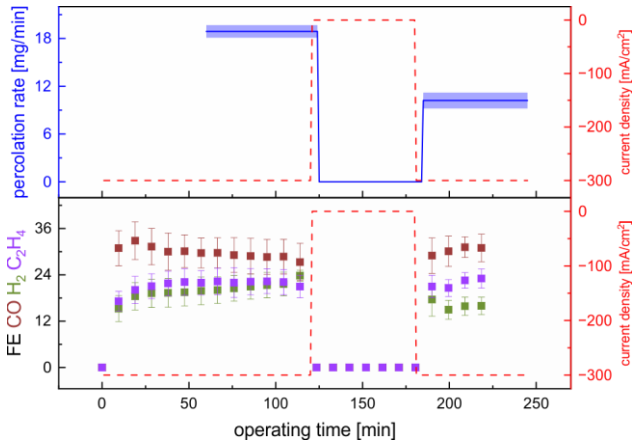

Figure 5 Temporal progression of gaseous product FEs and leakage rates under current pulses with current density alternating between 0 mA cm^{-2} (OCV) and 300 mA cm^{-2} during CO_2 electrolysis. Each experiment is repeated twice, with error bars to indicate the standard deviation. The OCV time period counteracted GDE flooding and prolonged the system´s lifetime.

Figure 5 shows that GDE leakage completely stops during the OCV period. This implies that GDE flooding is, at least, strongly reduced during the rest phase. However, the in-operando water trap cannot be used to determine whether the flooding of the GDE has been completely stopped, as the amount of electrolyte flowing through the GDE is measured, but not whether

the flooding takes place exclusively within the GDE. In situ methods such as neutron imaging would be necessary to determine whether flooding still occurs during OCV[24].

A comparison of the two segments before and after OCV shows that not only the percolation rate but also the FE_{H2} are higher before OCV than afterwards. One possible explanation could be that species damaging the GDE (e.g. liquid products or $KHCO_3$) are removed from the electrode during the OCV period, consequently restoring hydrophobicity and reducing leakage rates. This would suggest that the damaging species can accumulate in the electrode during electrolysis, since diffusion into the electrolyte does not occur fast enough. This confirms also the finding of Xu *et al.,* who were able to significantly enhance their system´s lifetime with a regeneration period by alternating the cell voltage. The regeneration period allowed carbonate ions to electromigrate to the anode, consequently lowering the concentration at the cathode and avoiding damaging salt formation[33]. It is likely that a similar effect occurred during the OCV phase, but that the carbonate concentration was lowered by thermodynamic diffusion since the cathode was not polarized during the regeneration phase. Regarding the decrease in FE_{H2} after OCV, it appears that previously flooded regions in the CL became accessible for CO_2 conversion again. This is an interesting observation, since reducing the current density from 300 to 100 mA cm^{-2} did not show this effect (see Figure 4). A possible explanation could be that GDE flooding still takes place at 100 mA cm^{-2}, while the flooding is interrupted during the OCV and the CL areas can consequently be recovered by restoring the hydrophobicity. In-situ methods such as neutron imaging would be necessary to further investigate this hypothesis.

Overall, results from Figure 5 suggest that periodic OCV interruptions during the CO_2 electrolysis could counteract GDE flooding and consequently prolong the system´s lifetime. However, further investigations are needed to determine if continuous interruptions will keep prolonging the system´s lifetime.

Conclusions

In summary, a new easy-to-implement method for the simultaneous quantification of GDE flooding and gaseous products during CO_2 electroreduction was developed and introduced. Initial galvanostatic experiments show that GDE flooding is a time- and current density-dependent process that changes not only the FEs but also the leakage rate of

the liquid flow through the GDE as its degradation progresses. The carbonisation of the electrolyte, leading to the precipitation of carbonate salts within the GDE, was identified as a possible reason for GDE flooding, which becomes more pronounced with increasing current densities. However, leakage rates at changing current densities showed no direct dependency on the degradation state of the GDE, which underlines the complexity behind the flooding phenomena. It was also found that leakage rates alone cannot always characterize the flooding state of the GDE, so that an additional correlation with the FE_{H2} is necessary. Additional experiments with alternating current density suggest that regeneration phases, for example by intermittently applying OCV, have the potential to stop or greatly reduce flooding and even regain previously flooded catalyst regions for CO_2 conversion. Based on these findings and advantages already mentioned, it can be assumed that the in-operando water trap will help to accelerate the development of robust and selective GDEs for CO2RR.

References

1. H. Huang, Y. Xu and A. N. van den Pol, *Journal of Neurophysiology,* **106**(3), 1191–1202 (2011).
2. Hoesung Lee, Katherine Calvin, Dipak Dasgupta, Gerhard Krinner, Aditi Mukherji, Peter Thorne, Christopher Trisos, José Romero, Paulina Aldunce and Alexander C Ruane, *CLIMATE CHANGE 2023 Synthesis Report: Summary for Policymakers (*2024).
3. D. Wu, F. Jiao and Q. Lu, *ACS Catal.,* **12**(20), 12993–13020 (2022).
4. T. Jaster, A. Gawel, D. Siegmund, J. Holzmann, H. Lohmann, E. Klemm and U.-P. Apfel, *iScience,* **25**(4), 104010 (2022).
5. M. W. Schreiber, *Current Opinion in Electrochemistry,* **44,** 101438 (2024).
6. D. Wu, F. Jiao and Q. Lu, *ACS Catal.,* **12**(20), 12993–13020 (2022).
7. C.-T. Dinh, T. Burdyny, M. G. Kibria, A. Seifitokaldani, C. M. Gabardo, F. P. García de Arquer, A. Kiani, J. P. Edwards, P. de Luna, O. S. Bushuyev, C. Zou, R. Quintero-Bermudez, Y. Pang, D. Sinton and E. H. Sargent, *Science (New York, N.Y.),* **360**(6390), 783–787 (2018).

8. I. E. L. Stephens, K. Chan, A. Bagger, S. W. Boettcher, J. Bonin, E. Boutin, A. K. Buckley, R. Buonsanti, E. R. Cave, X. Chang, S. W. Chee, A. H. M. Da Silva, P. de Luna, O. Einsle, B. Endrődi, M. Escudero-Escribano, J. V. Ferreira de Araujo, M. C. Figueiredo, C. Hahn, K. U. Hansen, S. Haussener, S. Hunegnaw, Z. Huo, Y. J. Hwang, C. Janáky, B. S. Jayathilake, F. Jiao, Z. P. Jovanov, P. Karimi, M. T. M. Koper, K. P. Kuhl, W. H. Lee, Z. Liang, X. Liu, S. Ma, M. Ma, H.-S. Oh, M. Robert, B. R. Cuenya, J. Rossmeisl, C. Roy, M. P. Ryan, E. H. Sargent, P. Sebastián-Pascual, B. Seger, L. Steier, P. Strasser, A. S. Varela, R. E. Vos, X. Wang, B. Xu, H. Yadegari and Y. Zhou, *J. Phys. Energy,* **4**(4), 42003 (2022).
9. D. Ren, J. Gao, S. M. Zakeeruddin and M. Grätzel, *J. Phys. Chem. Lett.,* **12**(31), 7583–7589 (2021).
10. S. Hernandez-Aldave and E. Andreoli, *Catalysts,* **10**(6), 713 (2020).
11. H. Shin, K. U. Hansen and F. Jiao, *Nat Sustain,* **4**(10), 911–919 (2021).
12. M. Li, M. N. Idros, Y. Wu, T. Burdyny, S. Garg, X. S. Zhao, G. Wang and T. E. Rufford, *J. Mater. Chem. A,* **9**(35), 19369–19409 (2021).
13. E. R. Cofell, U. O. Nwabara, S. S. Bhargava, D. E. Henckel and P. J. A. Kenis, *ACS applied materials & interfaces,* **13**(13), 15132–15142 (2021).
14. B. Sahin, M. Kraehling, V. Facci Allegrini, J. Leung, K. Wiesner-Fleischer, E. Magori, R. Pastusiak, A. Tawil, T. Hodges, E. Brooke, E. C. Corbos, M. Fleischer, E. Simon and O. Hinrichsen, *Journal of CO2 Utilization,* **82,** 102766 (2024).
15. L. M. Baumgartner, A. Goryachev, C. I. Koopman, D. Franzen, B. Ellendorff, T. Turek and D. A. Vermaas, *Energy Adv. (*2023).
16. B. de Mot, J. Hereijgers, M. Duarte and T. Breugelmans, *Chemical Engineering Journal,* **378,** 122224 (2019).
17. B. Sahin, S. Kimberly Raymond, F. Ntourmas, R. Pastusiak, K. Wiesner-Fleischer, M. Fleischer, E. Simon and O. Hinrichsen, *ACS applied materials & interfaces,* **15**(39), 45844–45854 (2023).
18. Z. Xing, L. Hu, D. S. Ripatti, X. Hu and X. Feng, *Nature communications,* **12**(1), 136 (2021).

19. D. A. Salvatore, D. M. Weekes, J. He, K. E. Dettelbach, Y. C. Li, T. E. Mallouk and C. P. Berlinguette, *ACS Energy Lett.,* **3**(1), 149–154 (2018).
20. Y. Wu, H. Rabiee, X. S. Zhao, G. Wang and Y. Jiang, *J. Mater. Chem. A,* **12**(24), 14206–14228 (2024).
21. C. P. O'Brien, D. McLaughlin, T. Böhm, Y. C. Xiao, J. P. Edwards, C. M. Gabardo, M. Bierling, J. Wicks, A. Sedighian Rasouli, J. Abed, D. Young, C.-T. Dinh, E. H. Sargent, S. Thiele and D. Sinton, *Joule,* **8**(10), 2903–2919 (2024).
22. Y. Kong, H. Hu, M. Liu, Y. Hou, V. Kolivoška, S. Vesztergom and P. Broekmann, *Journal of Catalysis,* **408,** 1–8 (2022).
23. P. Jeanty, C. Scherer, E. Magori, K. Wiesner-Fleischer, O. Hinrichsen and M. Fleischer, *Journal of CO2 Utilization,* **24,** 454–462 (2018).
24. J. Disch, L. Bohn, S. Koch, M. Schulz, Y. Han, A. Tengattini, L. Helfen, M. Breitwieser and S. Vierrath, *Nature communications,* **13**(1), 6099 (2022).
25. P. K. Sow, Z. Lu, H. Talebian, L. Damron and W. Mérida, *J. Phys. Chem. C,* **120**(43), 24794–24802 (2016).
26. G. O. Larrazábal, V. Okatenko, I. Chorkendorff, R. Buonsanti and B. Seger, *ACS applied materials & interfaces,* **14**(6), 7779–7787 (2022).
27. M. E. Leonard, L. E. Clarke, A. Forner-Cuenca, S. M. Brown and F. R. Brushett, *ChemSusChem,* **13**(2), 400–411 (2020).
28. T. J. Rabbow and A. H. Whitehead, *Carbon,* **111,** 782–788 (2017).
29. A. Reyes, R. P. Jansonius, B. A. W. Mowbray, Y. Cao, D. G. Wheeler, J. Chau, D. J. Dvorak and C. P. Berlinguette, *ACS Energy Lett.,* **5**(5), 1612–1618 (2020).
30. Y. Wu, S. Garg, M. Li, M. N. Idros, Z. Li, R. Lin, J. Chen, G. Wang and T. E. Rufford, *Journal of Power Sources,* **522,** 230998 (2022).
31. M. Wrobel, S. Kriescher, T. Schiffer, R. Keller and M. Wessling, *Chemical Engineering Journal,* **474,** 145335 (2023).
32. N. S. Romero Cuellar, K. Wiesner-Fleischer, M. Fleischer, A. Rucki and O. Hinrichsen, *Electrochimica Acta,* **307,** 164–175 (2019).

33. Y. Xu, J. P. Edwards, S. Liu, R. K. Miao, J. E. Huang, C. M. Gabardo, C. P. O'Brien, J. Li, E. H. Sargent and D. Sinton, *ACS Energy Lett.,* **6**(2), 809–815 (2021).